Supporting Information

Venturelli et al. 10.1073/pnas.1211902109

SI Text

S1. Distinguishing Dilution Memory from a History-Dependent Response. YFP is highly stable and predominantly decreases through cell dilution (1). As a consequence, activation of P_{GAL10} YFP is faster than deactivation and distributions of cells from high and low environments (E_H and E_L, respectively) will inevitably differ until cells equilibrate to a new steady state in the second set of environments (E_1, …, E_n). We estimated the amount of time, and hence the number of cell divisions, necessary to distinguish dilution memory from a history-dependent response (Fig. 2).

In the presence of 2% galactose, the steady-state YFP fluorescence expressed from the *GAL10* promoter was ∼78% of YFP fluorescence expressed from the *TDH3* promoter after autofluorescent background subtraction (Fig. S1*C*). There are ∼169,000 Tdh3 proteins present in glucose conditions in a haploid *Saccharomyces cerevisiae* background (2), corresponding to 131,820 Gal10 proteins (assuming promoter strength is proportional to the number of molecules). Therefore, the concentration of Gal10p is 7.5 μM at full galactose induction (3). As a lower bound, we assumed that 150 molecules of YFP (8.6 nM) were indistinguishable from the autofluorescence background using flow cytometry (4). Therefore, the number of cell divisions required to dilute YFP from full induction to background is $\log_2(7.5) - \log_2(0.0086) = 9.8$. In minimal dropout media supplemented with 2% raffinose, cells doubled approximately every 3 h during exponential phase, which corresponds to 30 h to distinguish dilution memory from a history-dependent response.

S2. Characterization of the *GAL3* Feedback Loop on the Bimodal Response. We found that bimodality persisted in the absence of the *GAL3* feedback loop for a range of WT *GAL3* levels, as shown in Fig. 3*A4*. These results are different from a previous study that attributed the observed bimodality of the galactose gene-regulatory network of *Saccharomyces cerevisiae* (GAL) to the activity of the *GAL3* feedback loop (5). This study used a diploid *GAL3* feedback loop deletion strain, where Gal3p was constitutively expressed with a *TET*-inducible promoter. Using fluorescent Gal3 fusion proteins, the authors identified 50 ng/mL doxycycline (dox) as equivalent to 80% of the WT *GAL3* levels induced with 0.5% galactose.

To explore the roles of the *GAL3* feedback loop on the bimodal response further, we repeated the experiments from the study by Acar et al. (5) using the MA0182 strain. Following the authors' protocol, we observed bimodality in P_{GAL1} YFP expression after an induction period of 27 h for 0.004% galactose in the absence of dox (Fig. S2*A*). A Gaussian mixture model was used to classify bimodality (*Materials and Methods*). Using this criterion, these data showed the *GAL3* feedback loop was not necessary for bimodality for some range of *GAL3* levels (Fig. S2*B*).

The galactose dose–response was next measured for different *GAL3* levels by inducing MA0182 with a range of galactose and dox concentrations (Fig. S2*A*). These data showed that MA0182 was bimodal for at least one galactose concentration between 0 and 25 ng/mL dox (Fig. S2*B*). However, bimodality was not detected for 50 ng/mL dox.

We compared *GAL3* mRNA levels with WT *GAL3* expression using real-time quantitative PCR. According to these results, 50 ng/mL dox corresponded to ∼150% *GAL3* levels relative to WT induced with 0.5% galactose (Fig. S2*C*). These results indicated that WT *GAL3* expression in MA0182 was between 0 ng/mL (36%) and ∼35 ng/mL (100%) dox. Acar et al. (5) stated that MA0182 displayed a graded response for 5–300% of *GAL3* levels with respect to WT. In our experiments, the lower bound for *GAL3* levels in MA0182 was 36% of maximal WT levels due to leakiness of the *TET*-inducible promoter system.

In summary, MA0182 exhibited a bimodal response for a range of WT *GAL3* expression levels and was graded when Gal3p was overexpressed. This transformation of the GAL dose–response from bimodal to graded by tuning the concentration of Gal3p corroborates the importance of comparing feedback loop KOs at similar operating point(s) to understand fully the contribution of these regulatory connections to a phenotype (6) (section S3).

S3. Comparison of Open and Closed Loop Transcriptional Circuits. In engineering, closed and open loop systems are frequently compared to determine the advantages of feedback control on performance (7). Similarly, in biology, a controlled comparison for open and closed loop systems may provide insight about the role of a feedback loop (6). One approach to creating the open loop system is to delete the gene involved in the loop. However, deleting a gene is an aggressive approach that may significantly shift the operating point of the circuit, making it difficult to attribute the changes in phenotype to the function of the feedback loop. Deleting the coding region of the gene involved in the loop and expressing this gene from a constitutive promoter is a superior approach for evaluating the function of a feedback loop. The constitutive promoter strength is an important parameter to adjust because a comparison of the open and closed loop systems should be made in the neighborhood of the WT equilibrium point(s).

Consider a bistable transcriptional circuit modeled by an ordinary differential equation (ODE) that has two stable steady states for a specific range of an input parameter, u: $\frac{dx}{dt} = u + H(x,\theta) - \gamma x$. We are interested in the role of a positive feedback loop of protein, x. In the closed loop system (WT), $H(x,\theta)$ represents transcriptional feedback regulation, where

$$H(x,\theta) = \frac{\alpha x^n}{x^n + K^n}.$$

For $u = u_1$, $\frac{dx}{dt} = 0 \Rightarrow x = x_{ei}$, where i corresponds to the particular equilibrium point ($i = 1, 2$ within the bistable parameter regime). Given $u = u_1$ in the bistable region, the open loop system should be evaluated at $\alpha_{OL1} = H(x_{e1},\theta)|_{u=u_1}$ and $\alpha_{OL2} = H(x_{e2},\theta)|_{u=u_1}$, where α_{OL1} and α_{OL2} represent the constitutive (open loop) production rates. Experimentally mapping the open and closed loop production rates for a range of inputs, $u = u_1, \ldots, u_n$, may be challenging due to a limited number of well-characterized constitutive promoters and restricted dynamic ranges of inducible promoter systems. To circumvent this, an intermediate α'_{OL} can be chosen within the WT expression range:

$$\alpha'_{OL} \in [H(\min(x_{ei}),\theta), H(\max(x_{ei}),\theta)] \text{ for } u_1, \ldots, u_n.$$

The caveat for this approximation is that α'_{OL} produces a higher and/or lower open loop expression level compared with WT for each value of u. Using this approach, it is therefore important to check that the role of the feedback does not depend on the specific value α'_{OL} by scanning several values within WT range (Figs. S2 and S4).

S4. Model Description and Steady-State Solution. An ODE model of the GAL gene-regulatory circuit was constructed based on the

interactions shown in Fig. 1. This model was able to provide explanations for experimental data and insights about the interplay of feedback loops. The following simplifications were made to the model: intracellular galactose concentration was constant, Gal2p was excluded because the *GAL2* feedback is not necessary for bimodality (Fig. 3*B1*), no distinction was made between Gal1p, Gal1p bound to galactose (Gal1p*), and Gal3p, Gal3 bound to galactose (Gal3p*), because both the galactose-bound and unbound forms can lead to GAL gene induction (8), nuclear and cytoplasmic partitioning of the GAL proteins was not included because this is a subject of debate (9–11), and dimerization of Gal4p and Gal80p was not modeled (12, 13).

The following simplifications were made to the model: (*i*) intracellular galactose concentration was constant, (*ii*) Gal2p was excluded because the *GAL2* feedback is not necessary for bimodality (Fig. 3 *B1*), (*iii*) no distinction was made between Gal1p, Gal1p bound to galactose (Gal1p*), and Gal3p, Gal3 bound to galactose because both the galactose-bound and unbound forms can lead to GAL gene induction (8), (*iv*) nuclear and cytoplasmic partitioning of the GAL proteins was not included because this is a subject of debate (9–11), and (*v*) dimerization of Gal4p and Gal80p was not modeled (12, 13).

For constant galactose concentrations, conversion of Gal1p, Gal3p into Gal1p*, Gal3p* is a first-order reaction. This first-order reaction was approximated as a zeroth-order reaction using galactose at a constant input rate (α_{gal}). The protein concentrations of Gal1p (G1), Gal3p (G3), Gal4p (G4), and Gal80p (G80) were modeled. The Hill coefficients for G1 (n_1), G3 (n_3), and G80 (n_{80}) were estimated as 3, 2, and 2, respectively, based on experimental measurements (Fig. S1*D*).

Based on these assumptions, the model that captures the set of critical molecular interactions for bistability in the WT GAL network is

$$\frac{d[\mathrm{G1}]}{dt} = \epsilon\alpha_{gal} + \alpha_{G1}\left(\frac{[\mathrm{G4}]^{n_1}}{K_{G1}^{n_1} + [\mathrm{G4}]^{n_1}}\right) - k_{f81}[\mathrm{G1}][\mathrm{G80}] + k_{r81}[\mathrm{C81}] - \gamma_{G1}[\mathrm{G1}],$$

$$\frac{d[\mathrm{G3}]}{dt} = \alpha_{gal} + \alpha_{G3}\left(\frac{[\mathrm{G4}]^{n_3}}{K_{G3}^{n_3} + [\mathrm{G4}]^{n_3}}\right) - k_{f83}[\mathrm{G3}][\mathrm{G80}] + k_{r83}[\mathrm{C83}] - \gamma_{G3}[\mathrm{G3}],$$

$$\frac{d[\mathrm{G4}]}{dt} = \alpha_{G4} - k_{f84}[\mathrm{G4}][\mathrm{G80}] + k_{r84}[\mathrm{C84}] - \gamma_{G4}[\mathrm{G4}],$$

$$\frac{d[\mathrm{G80}]}{dt} = \alpha_{oG80} + \alpha_{G80}\left(\frac{[\mathrm{G4}]^{n_{80}}}{K_{G80}^{n_{80}} + [\mathrm{G4}]^{n_{80}}}\right) - k_{f81}[\mathrm{G1}][\mathrm{G80}] + k_{r81}[\mathrm{C81}] - k_{f83}[\mathrm{G3}][\mathrm{G80}] + k_{r83}[\mathrm{C83}] - k_{f84}[\mathrm{G4}][\mathrm{G80}] + k_{r84}[\mathrm{C84}] - \gamma_{G80}[\mathrm{G80}],$$

$$\frac{d[\mathrm{C81}]}{dt} = k_{f81}[\mathrm{G1}][\mathrm{G80}] - k_{r81}[\mathrm{C81}] - \gamma_{C81}[\mathrm{C81}],$$

$$\frac{d[\mathrm{C83}]}{dt} = k_{f83}[\mathrm{G3}][\mathrm{G80}] - k_{r83}[\mathrm{C83}] - \gamma_{C83}[\mathrm{C83}],$$

$$\frac{d[\mathrm{C84}]}{dt} = k_{f84}[\mathrm{G4}][\mathrm{G80}] - k_{r84}[\mathrm{C84}] - \gamma_{C84}[\mathrm{C84}].$$

Using the quasi–steady-state assumption, the concentrations of the complexes Gal1p-Gal80p (C81), Gal3p-Gal80p (C83), and Gal4p-Gal80p (C84) reached their respective equilibria significantly faster than the dynamics of G1, G3, G4, and G80, $\left(\frac{d[\mathrm{C81}]}{dt} = \frac{d[\mathrm{C83}]}{dt} = \frac{d[\mathrm{C84}]}{dt} = 0\right)$, yielding

$$[\mathrm{C81}] = \frac{k_{f81}[\mathrm{G1}][\mathrm{G80}]}{k_{r81} + \gamma_{C81}}, \quad [\mathrm{C83}] = \frac{k_{f83}[\mathrm{G3}][\mathrm{G80}]}{k_{r83} + \gamma_{C83}},$$

$$[\mathrm{C84}] = \frac{k_{f84}[\mathrm{G4}][\mathrm{G80}]}{k_{r84} + \gamma_{C84}}.$$

This assumption was used to simplify the system of equations to the following four ODEs:

$$\frac{d[\mathrm{G1}]}{dt} = \alpha_{gal}\epsilon + \alpha_{G1}\left(\frac{[\mathrm{G4}]^{n_1}}{K_{G1}^{n_1}[\mathrm{G4}]^{n_1}}\right) + \omega[\mathrm{G1}][\mathrm{G80}] - \gamma_{G1}[\mathrm{G1}],$$

$$\frac{d[\mathrm{G3}]}{dt} = \alpha_{gal} + \alpha_{G3}\left(\frac{[\mathrm{G4}]^{n_3}}{K_{G3}^{n_3} + [\mathrm{G4}]^{n_3}}\right) + \delta[\mathrm{G3}][\mathrm{G80}] - \gamma_{G3}[\mathrm{G3}],$$

$$\frac{d[\mathrm{G4}]}{dt} = \alpha_{G4} + \beta[\mathrm{G80}][\mathrm{G4}] - \gamma_{G4}[\mathrm{G4}],$$

$$\frac{d[\mathrm{G80}]}{dt} = \alpha_{oG80} + \alpha_{G80}\left(\frac{[\mathrm{G4}]^{n_{80}}}{K_{G80}^{n_{80}} + [\mathrm{G4}]^{n_{80}}}\right) + \omega[\mathrm{G1}][\mathrm{G80}] + \delta[\mathrm{G3}][\mathrm{G80}] + \beta[\mathrm{G80}][\mathrm{G4}] - \gamma_{G80}[\mathrm{G80}],$$

where

$$\omega = \frac{k_{r81}k_{f81}}{k_{r81} + \gamma_{C81}} - k_{f81}, \quad \delta = \frac{k_{r83}k_{f83}}{k_{r83} + \gamma_{C83}} - k_{f83},$$

$$\beta = \frac{k_{r84}k_{f84}}{k_{r84} + \gamma_{C84}} - k_{f84}.$$

At steady state, $\frac{d[\mathrm{G1}]}{dt} = \frac{d[\mathrm{G3}]}{dt} = \frac{d[\mathrm{G4}]}{dt} = \frac{d[\mathrm{G80}]}{dt} = 0$ and the equilibrium concentrations are

$$\mathrm{G1}_e = \frac{-\epsilon\alpha_{gal} - H_{G1}(\mathrm{G4}_e, \theta_{G1})}{\omega\mathrm{G80}_e - \gamma_{G1}},$$

$$\mathrm{G3}_e = \frac{-\alpha_{gal} - H_{G3}(\mathrm{G4}_e, \theta_{G3})}{\delta\mathrm{G80}_e - \gamma_{G1}},$$

$$\mathrm{G80}_e = \frac{-\alpha_{G4} + \gamma_{G4}\mathrm{G4}_e}{\beta\mathrm{G4}_e},$$

where $\mathrm{G1}_e$, $\mathrm{G3}_e$, $\mathrm{G4}_e$, and $\mathrm{G80}_e$ are the equilibrium values of G1, G3, G80, and G4, respectively. $\mathrm{G4}_e$ was determined by computing the roots of a 11th-order polynomial

$$a_0 + a_1\mathrm{G4}_e + \ldots + a_{11}\mathrm{G4}_e^{11} = 0,$$

where the coefficients, a_i, are functions of the model parameters. The *GAL1*, *GAL3*, and *GAL80* feedback deletion models listed in section S6 were solved by applying the same procedure. The stability of the equilibrium points was determined by computing the eigenvalues of the Jacobian matrix of the system of equations (7).

S5. Estimation of Model Parameters. ***S5.1. Parameter set I.*** Parameters for the model were estimated from experimental measurements and previous studies (Table S1). *GAL1* and *GAL10* share a bidirectional promoter ($P_{GAL1\text{-}10}$). As a consequence, these genes exhibit highly similar galactose induction responses.

The *GAL3* and *GAL80* promoters each have a single Gal4p binding site and are produced at a basal rate in the absence of galactose. Multiple Gal4p binding sites in the *GAL2*, *GAL7*, and *GAL1–10* promoters stabilize Gal80p dimers on DNA, augmenting the strength of repression and the maximum production rate (14). As a result, promoters with multiple Gal4p binding sites have a significantly larger dynamic range of expression.

Flow cytometry measurements of *GAL3*, *GAL10*, and *GAL80* promoter fusions to Venus in response to galactose were used to compare relative promoter strengths and cooperativity. The *GAL3* (P_{GAL3}) and *GAL80* (P_{GAL80}) promoter fusions (P_{GAL3} Venus and P_{GAL80} Venus) exhibited a graded response, whereas the *GAL10* promoter fusion had a bimodal response, as shown in Fig. 3*A1*. The Hill coefficients for the Gal4p-dependent feedback terms were approximated by fitting the means of the graded response distributions (M_Y; *Materials and Methods*) and the fraction of high expressing cells for the bimodal response (P_{GAL10}) to Hill functions.

A Hill function fit to the means of the distributions for P_{GAL3} Venus and P_{GAL80} Venus in response to galactose generated Hill coefficients of 2.2 and 2, respectively. Gal4p binds to DNA as a dimer and has been shown to interact cooperatively (12, 15). Based on these results, we assumed that the Hill coefficients for the *GAL3* and *GAL80* transcriptional feedback terms were both 2 (12, 15).

Fitting the fraction of high expression cells for P_{GAL10} produced a Hill coefficient of ~3.2. The *GAL1–10* promoter has four Gal4p binding sites, which have been shown to increase cooperativity. Therefore, we set the Hill coefficient of the *GAL1* feedback to 3 (15). We note that the main conclusions about the roles of the *GAL1*, *GAL3*, and *GAL80* feedback loops do not change if the Hill coefficients of the feedback terms for Gal1p, Gal3p, and Gal80p are set to 4, 1, and 1 or to 3, 1, and 1.

The constitutive and feedback production rates were approximated using the number of proteins per cell (2). Gal4p is weakly expressed, and its constitutive production rate (α_{G4}) was selected to reflect this observation (16). The mean expression levels for P_{GAL3} Venus and P_{GAL80} Venus were similar in response to galactose, as shown in Fig. S1*E*. At saturation (0.1% galactose), P_{GAL80} Venus was approximately 15% higher than P_{GAL3} Venus. The production rates, α_{G3}, α_{G80}, and α_{oG80}, were chosen to have similar ratios to mirror the experimental measurements. Because Gal1p has been shown to bind to Gal80p with lower affinity than Gal3p, a scaling factor of ε was used to modify α_{gal} (17, 18).

Forward binding rates (k_{f83}, k_{f81}, and k_{f84}) were estimated using the limits of diffusion. The dissociation rates (k_{r83}, k_{r81}, and k_{r84}) were free parameters with the requirement that $k_{r81} \gg k_{r83}$ (17, 18). All proteins were assumed to degrade at the rate of cell division.

S5.2. Parameter set II. To identify parameter sets that qualitatively matched the previously reported dynamic switch response of Gal1p and Gal3p (19), 10,000 parameter sets were sampled uniformly in linear scale in the 22-dimensional parameter space, using the Latin hypercube sampling method (20). The following parameter ranges were used: 10–160 $(\text{nM}\cdot\text{min})^{-1}$ for the forward binding constants (k_{f81}, k_{f83}, and k_{f84}); 1–5,000 min^{-1} for the dissociation constants (k_{f81}, k_{f83}, and k_{f84}); 0.0035–0.06 min^{-1} for the degradation rates (γ_{G1}, γ_{G3}, γ_{G80}, γ_{G4}, γ_{C81}, γ_{C83}, and γ_{C84}); 0.01–100 nM for the EC_{50} values in the Hill functions (K_{G1}, K_{G3}, and K_{G80}); 0.1–40 $\text{nM}\cdot\text{min}^{-1}$ for α_{G1} ; 0.1–10 $\text{nM}\cdot\text{min}^{-1}$ for α_{G3}, α_{oG80}, and α_{G80}; 0.1–5 $\text{nM}\cdot\text{min}^{-1}$ for α_{G4}; and 0.01–2 for ε. The constitutive rates for the feedback KOs were fixed at 0.1, 0.1, and 1.5 $\text{nM}\cdot\text{min}^{-1}$ for α_{G1s}, α_{G3s}, and α_{G80s}, respectively. The hysteresis strength, D_H, was computed for each parameter set and for each of the five models including WT and feedback deletions of GAL1, GAL3, GAL80 and the double GAL1 and GAL3 feedback deletion. First, these parameter sets were filtered based on the presence of bistability. Second, the subsets of parameter sets that satisfied these constraints were simulated and the relative concentrations of C81 and C83 were calculated at initial (10 min) and delayed (500 min) time points by simulation of the full WT model before applying the quasi–steady-state assumption.

S6. Feedback Loop Deletion Models. The individual *GAL1*, *GAL3*, and *GAL80* feedback deletions and the combined *GAL1* and *GAL3* feedback deletion were obtained by replacing the appropriate Hill functions representing transcriptional regulation by Gal4p with a constant. In the GAL80Δ fb model, the basal and constitutive production rates were lumped into one parameter, α_{G80s}. The GAL1Δ GAL3Δ fb model was obtained from the GAL1Δ fb GAL3Δ fb model by setting $\alpha_{G1s} = 0$ and $\epsilon = 0$. The set of ODEs to model the five feedback loop KO topologies are provided in the following sections.

S6.1. GAL1 feedback deletion (GAL1Δ fb).

$$\frac{d[\text{G1}]}{dt} = \epsilon\alpha_{gal} + \alpha_{G1s} + \omega[\text{G1}][\text{G80}] - \gamma_{G1}[\text{G1}],$$

$$\frac{d[\text{G3}]}{dt} = \alpha_{gal} + \alpha_{G3}\left(\frac{[\text{G4}]^2}{K_{G3}^2 + [\text{G4}]^2}\right) + \delta[\text{G3}][\text{G80}] - \gamma_{G3}[\text{G3}],$$

$$\frac{d[\text{G4}]}{dt} = \alpha_{G4} + \beta[\text{G80}][\text{G4}] - \gamma_{G4}[\text{G4}],$$

$$\frac{d[\text{G80}]}{dt} = \alpha_{oG80} + \alpha_{G80}\left(\frac{[\text{G4}]^2}{K_{G80}^2 + [\text{G4}]^2}\right) + \omega[\text{G1}][\text{G80}] + \delta[\text{G3}][\text{G80}] + \beta[\text{G80}][\text{G4}] - \gamma_{G80}[\text{G80}].$$

S6.2. GAL3 feedback deletion (GAL3Δ fb).

$$\frac{d[\text{G1}]}{dt} = \epsilon\alpha_{gal} + \alpha_{G1}\left(\frac{[\text{G4}]^3}{K_{G1}^3 + [\text{G4}]^3}\right) + \omega[\text{G1}][\text{G80}] - \gamma_{G1}[\text{G1}],$$

$$\frac{d[\text{G3}]}{dt} = \alpha_{gal} + \alpha_{G3s} + \delta[\text{G3}][\text{G80}] - \gamma_{G3}[\text{G3}],$$

$$\frac{d[\text{G4}]}{dt} = \alpha_{G4} + \beta[\text{G80}][\text{G4}] - \gamma_{G4}[\text{G4}],$$

$$\frac{d[\text{G80}]}{dt} = \alpha_{oG80} + \alpha_{G80}\left(\frac{[\text{G4}]^2}{K_{G80}^2 + [\text{G4}]^2}\right) + \omega[\text{G1}][\text{G80}] + \delta[\text{G3}][\text{G80}] + \beta[\text{G80}][\text{G4}] - \gamma_{G80}[\text{G80}].$$

S6.3. GAL80 feedback deletion (GAL80Δ fb).

$$\frac{d[\text{G1}]}{dt} = \epsilon\alpha_{gal} + \alpha_{G1}\left(\frac{[\text{G4}]^3}{K_{G1}^3 + [\text{G4}]^3}\right) + \omega[\text{G1}][\text{G80}] - \gamma_{G1}[\text{G1}],$$

$$\frac{d[\text{G3}]}{dt} = \alpha_{gal} + \alpha_{G3}\left(\frac{[\text{G4}]^2}{K_{G3}^2 + [\text{G4}]^2}\right) + \delta[\text{G3}][\text{G80}] - \gamma_{G3}[\text{G3}],$$

$$\frac{d[\text{G4}]}{dt} = \alpha_{G4} + \beta[\text{G80}][\text{G4}] - \gamma_{G4}[\text{G4}],$$

$$\frac{d[\mathrm{G80}]}{dt} = \alpha_{G80s} + \omega[\mathrm{G1}][\mathrm{G80}] + \delta[\mathrm{G3}][\mathrm{G80}] + \beta[\mathrm{G80}][\mathrm{G4}] - \gamma_{G80}[\mathrm{G80}].$$

S6.4. GAL1 and GAL3 feedback deletions (GAL1Δ fb GAL3Δ fb).

$$\frac{d[\mathrm{G1}]}{dt} = \epsilon\alpha_{gal} + \alpha_{G1s} + \omega[\mathrm{G1}][\mathrm{G80}] - \gamma_{G1}[\mathrm{G1}],$$

$$\frac{d[\mathrm{G3}]}{dt} = \alpha_{gal} + \alpha_{G3s} + \delta[\mathrm{G3}][\mathrm{G80}] - \gamma_{G3}[\mathrm{G3}],$$

$$\frac{d[\mathrm{G4}]}{dt} = \alpha_{G4} + \beta[\mathrm{G80}][\mathrm{G4}] - \gamma_{G4}[\mathrm{G4}],$$

$$\frac{d[\mathrm{G80}]}{dt} = \alpha_{oG80} + \alpha_{G80}\left(\frac{[\mathrm{G4}]^2}{K_{G80}^2 + [\mathrm{G4}]^2}\right) + \omega[\mathrm{G1}][\mathrm{G80}] + \delta[\mathrm{G3}][\mathrm{G80}] + \beta[\mathrm{G80}][\mathrm{G4}] - \gamma_{G80}[\mathrm{G80}].$$

S7. General Models of Molecular Sequestration with Positive Feedback. We constructed generalizable models of molecular sequestration with positive feedback to examine the relationship between the binding affinity of the activator-repressor pair(s) and the system's region of bistability. We first explored the parameter dependence of a simple model of an activator x that is regulated by a transcriptional repressor z with a Hill coefficient of 1 (noncooperative). In this model, x can sequester z to form an inactive heterodimer, hence generating a positive feedback loop.

Next, we analyzed the steady-state and dynamic properties of systems with two activators, x_1 and x_2, that are each regulated by the transcriptional repressor z and can sequester z into two inactive complexes (c_1 and c_2), thus forming one or two positive feedback loops. In these models, the mechanisms of sequestration and positive feedback are triggered by an input (u) that represents a basal production rate of x, x_1, and x_2.

S7.1. Model description for single noncooperative sequestration feedback loop. The three equations that implement a single noncooperative sequestration feedback loop (Fig. 8 *A* and *B*) are

$$\frac{dx}{dt} = u + \frac{\alpha K}{K + z} - k_f x z + k_r c - \gamma_x x,$$

$$\frac{dc}{dt} = k_f x z - k_r c - \gamma_c c,$$

$$\frac{dz}{dt} = \alpha_z - k_f x z + k_r c - \gamma_z z.$$

Here, u represents the input. Assuming that $\frac{dc}{dt} = 0$ (quasi–steady-state approximation), the model was reduced to

$$\frac{dx}{dt} = u + \frac{\alpha K}{K + z} + \beta x z - \gamma_x x,$$

$$\frac{dz}{dt} = \alpha_z + \beta x z - \gamma_z z,$$

where $\beta = k_f\left(\frac{k_r}{k_r + \gamma_c} - 1\right)$. The parameter values were set to $\alpha_x = 5$ nM·min^{-1}, $\alpha_z = 10$ nM·min^{-1}, $\gamma_x = \gamma_c = \gamma_z = 0.005$ min^{-1}, $K = 100$ nM, and $k_f = 100$ nM·min^{-1}. The values for u and k_r varied within the range of 0.1–10 nM·min^{-1} and 0.1–1,000 min^{-1} (Fig. S8*B*). A bifurcation analysis was performed by computing the roots of the cubic polynomial in z.

S7.2. Model description for double sequestration linked feedback loops. The ODE model that represents a double sequestration linked feedback loop system, as shown in Fig. 6*A*, consists of the following equations:

$$\frac{dx_1}{dt} = u + \frac{\alpha_1 K_1^3}{K_1^3 + z^3} - k_{f1} x_1 z + k_{r1} c_1 - \gamma_1 x_1,$$

$$\frac{dx_2}{dt} = u + \frac{\alpha_2 K_2^2}{K_2^2 + z^2} - k_{f2} x_2 z + k_{r2} c_2 - \gamma_2 x_2,$$

$$\frac{dc_1}{dt} = k_{f1} x_1 z - k_{r1} c_1 - \gamma_{c1} c_1,$$

$$\frac{dc_2}{dt} = k_{f2} x_2 z - k_{r2} c_2 - \gamma_{c2} c_2,$$

$$\frac{dz}{dt} = \alpha_z - k_{f1} x_1 z + k_{r1} c_1 - k_{f2} x_2 z + k_{r2} c_2 - \gamma_z z.$$

Here, u represents the input. Assuming the inactive complexes (c_1 and c_2) approach equilibrium significantly faster than the other species (quasi–steady-state approximation), the system of equations was reduced to

$$\frac{dx_1}{dt} = u + \frac{\alpha_1 K_1^3}{K_1^3 + z^3} + \beta_1 x_1 z - \gamma_1 x_1,$$

$$\frac{dx_2}{dt} = u + \frac{\alpha_2 K_2^2}{K_2^2 + z^2} + \beta_2 x_2 z - \gamma_2 x_2,$$

$$\frac{dz}{dt} = \alpha_z + \beta_1 x_1 z + \beta_2 x_2 z - \gamma_z z,$$

where $\beta_1 = k_{f1}\left(\frac{k_{r1}}{k_{r1} + \gamma_{c1}} - 1\right)$ and $\beta_2 = k_{f2}\left(\frac{k_{r2}}{k_{r2} + \gamma_{c2}} - 1\right)$.

The parameter values were set to $\alpha_1 = \alpha_2 = 5$ nM·min^{-1}, $\alpha_z = 10$ nM·min^{-1}, $\gamma_1 = \gamma_2 = \gamma_{c1} = \gamma_{c2} = \gamma_z = 0.005$ min^{-1}, $K_1 = K_2 = 100$ nM, and $k_{f1} = k_{f2} = 100$ nM·min^{-1}. The values of u, k_{r1}, and k_{r2} were each varied over a range of values. The single feedback loop models referred to as the "single $n_{\mathrm{Hill}} = 2$" and the "single $n_{\mathrm{Hill}} = 3$" were obtained by replacing the Hill functions by a constitutive production rate, α_{1s} or α_{2s}. These parameters were set to $\alpha_{1s} = 5$ nM·min^{-1}, $\alpha_{2s} = 5$ nM·min^{-1} or $\alpha_{1s} = 0.1$ nM·min^{-1}, $\alpha_{2s} = 0.1$ nM·min^{-1} for the activation or deactivation response time analysis, respectively (see below). A bifurcation analysis was performed by calculating the roots of polynomials in z. The dual, single $n_{\mathrm{Hill}} = 2$, and single $n_{\mathrm{Hill}} = 3$ models were simplified to seventh-, fifth-, and sixth-order polynomials in z, respectively.

Response time analysis. The activation and deactivation response times were computed by simulation of the full sequestration models described above before applying the quasi–steady-state approximation (six-state ODE model, including an output species, z). Total simulation time was 5,000 min. The equation for the output species was

$$\frac{dy}{dt} = \frac{\alpha_y K_y^3}{K_y^3 + z^3} - \gamma_y y,$$

and the parameters equaled $\alpha_y = 10$ nM·min^{-1}, $K_y = 100$ nM, and $\gamma_y = 0.005$ min^{-1}.

Activation response times. For the activation time simulations, $u = 0$ for $t \leq 500$ min and then $u = 10$ for $t > 500$ min. The initial conditions approximated the steady-state concentrations for the low state, where $x_{1o} = 0.005$ nM, $x_{2o} = 0.01$ nM, $c_{1o} = 0.12$ nM, $c_{2o} = 2.4$ nM, $z_o = 1{,}998$ nM, and $y_o = 0.26$ nM. The time required for y (normalized between 0 and 1) to increase to half of its maximum value was computed for each set of K_{D1} and K_{D2} values. In the single feedback loop models, the constitutive production rates of x_1 or x_2 (α_{1s} or α_{2s}) were set to 0.1 nM·min^{-1} because this value approximated the Hill functions at equilibrium for $u = 0$.

Deactivation response times. For the deactivation time simulations, $u = 10$ for $t \leq 500$ min and then $u = 0$ for $t > 500$ min. The initial conditions approximated the steady-state concentrations for the high state, where $x_{1o} = 1{,}943$ nM, $x_{2o} = 1{,}891$ nM, $c_{1o} = 993$ nM, $c_{2o} = 966$ nM, $z_o = 40.9$ nM, and $y_o = 1872$ nM. The time required for z (normalized between 0 and 1) to decay to half of its maximum value was computed for each set of K_{D1} and K_{D2} values. In the single feedback loop models, the constitutive production rates of x_1 or x_2 (α_{1s} or α_{2s}) were set to 5 nM·min^{-1} because this value approximated the Hill functions at equilibrium for $u = 10$.

1. Mateus C, Avery SV (2000) Destabilized green fluorescent protein for monitoring dynamic changes in yeast gene expression with flow cytometry. *Yeast* 16(14): 1313–1323.
2. Huh WK, et al. (2003) Global analysis of protein localization in budding yeast. *Nature* 425(6959):686–691.
3. Tyson CB, Lord PG, Wheals AE (1979) Dependency of size of *Saccharomyces cerevisiae* cells on growth rate. *J Bacteriol* 138(1):92–98.
4. Newman JR, et al. (2006) Single-cell proteomic analysis of *S. cerevisiae* reveals the architecture of biological noise. *Nature* 441(7095):840–846.
5. Acar M, Becskei A, van Oudenaarden A (2005) Enhancement of cellular memory by reducing stochastic transitions. *Nature* 435(7039):228–232.
6. Savageau M (1976) *Biochemical Systems Analysis* (Addison–Wesley, Reading, MA).
7. Aström K, Murray R (2008) *Feedback Systems: An Introduction for Scientists and Engineers* (Princeton Univ Press, Princeton).
8. Bhat PJ, Hopper JE (1992) Overproduction of the GAL1 or GAL3 protein causes galactose-independent activation of the GAL4 protein: Evidence for a new model of induction for the yeast GAL/MEL regulon. *Mol Cell Biol* 12(6):2701–2707.
9. Peng G, Hopper JE (2000) Evidence for Gal3p's cytoplasmic location and Gal80p's dual cytoplasmic-nuclear location implicates new mechanisms for controlling Gal4p activity in *Saccharomyces cerevisiae*. *Mol Cell Biol* 20(14):5140–5148.
10. Wightman R, Bell R, Reece RJ (2008) Localization and interaction of the proteins constituting the GAL genetic switch in *Saccharomyces cerevisiae*. *Eukaryot Cell* 7(12): 2061–2068.
11. Egriboz O, Jiang F, Hopper JE (2011) Rapid GAL gene switch of *Saccharomyces cerevisiae* depends on nuclear Gal3, not nucleocytoplasmic trafficking of Gal3 and Gal80. *Genetics* 189(3):825–836.
12. Hong M, et al. (2008) Structural basis for dimerization in DNA recognition by Gal4. *Structure* 16(7):1019–1026.
13. Pilauri V, Bewley M, Diep C, Hopper J (2005) Gal80 dimerization and the yeast GAL gene switch. *Genetics* 169(4):1903–1914.
14. Melcher K, Xu HE (2001) Gal80-Gal80 interaction on adjacent Gal4p binding sites is required for complete GAL gene repression. *EMBO J* 20(4):841–851.
15. Giniger E, Ptashne M (1988) Cooperative DNA binding of the yeast transcriptional activator GAL4. *Proc Natl Acad Sci USA* 85(2):382–386.
16. Griggs DW, Johnston M (1993) Promoter elements determining weak expression of the GAL4 regulatory gene of *Saccharomyces cerevisiae*. *Mol Cell Biol* 13(8):4999–5009.
17. Timson DJ, Ross HC, Reece RJ (2002) Gal3p and Gal1p interact with the transcriptional repressor Gal80p to form a complex of 1:1 stoichiometry. *Biochem J* 363(Pt 3): 515–520.
18. Johnston M (1987) A model fungal gene regulatory mechanism: The GAL genes of *Saccharomyces cerevisiae*. *Microbiol Rev* 51(4):458–476.
19. Abramczyk D, Holden S, Page CJ, Reece RJ (2012) Interplay of a ligand sensor and an enzyme in controlling expression of the *Saccharomyces cerevisiae* GAL genes. *Eukaryot Cell* 11(3):334–342.
20. Iman R, Davenport J, Zeigler D (1980) *Latin Hypercube Sampling Program Users Guide* (Sandia Labs, Alburquerque, NM).

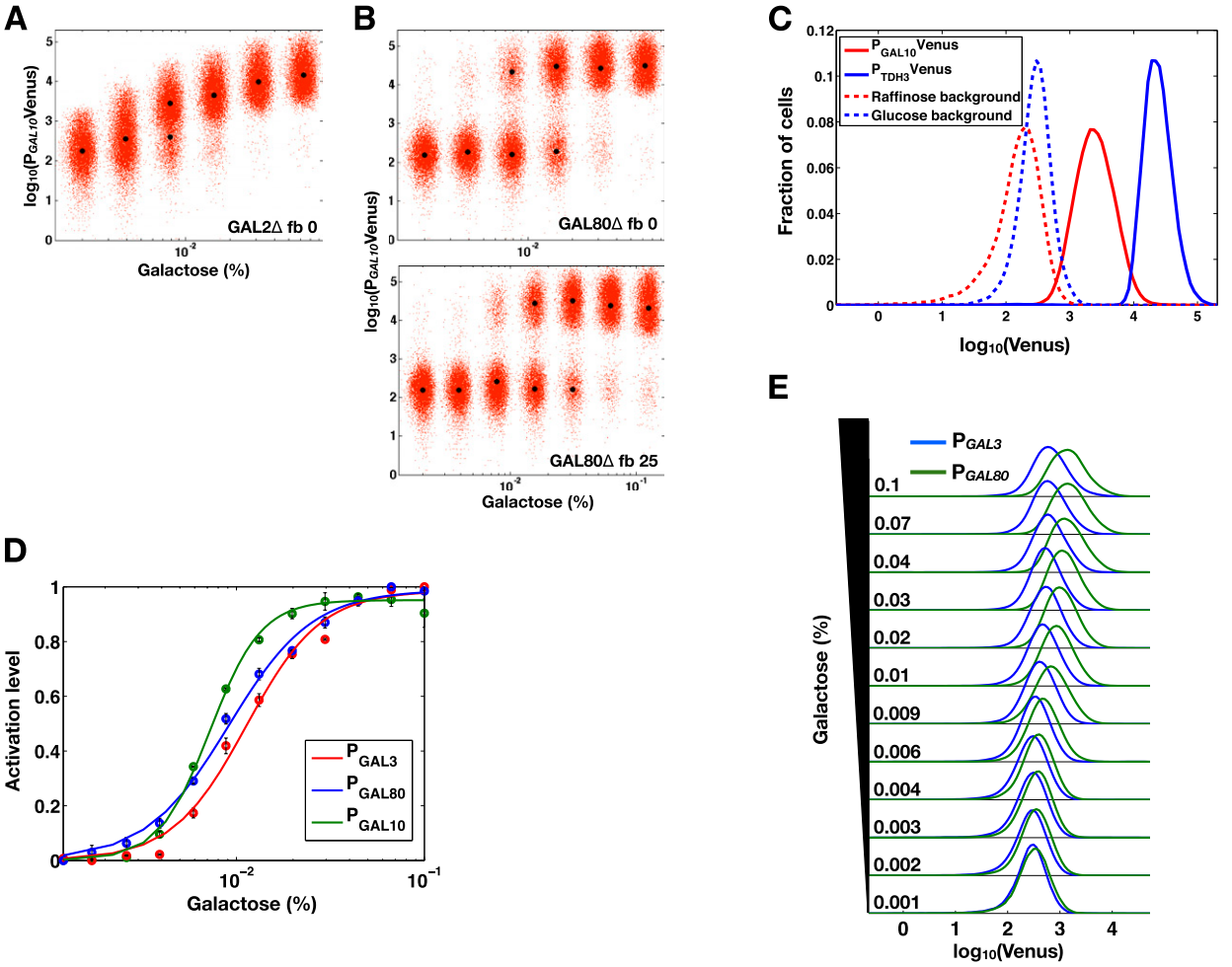

Fig. S1. Characterization of dose responses, promoter strengths, and ultrasensitivity. Bimodality persists in the absence of the individual *GAL2* and *GAL80* feedback loops for a wide range of constitutive *GAL2* and *GAL80* levels. Venus (YFP) fusions to the *TDH3*, *GAL3*, *GAL10*, and *GAL80* promoters in a WT background (P_{TDH3} Venus, P_{GAL3} Venus, P_{GAL10} Venus, and P_{GAL80} Venus). (*A*) *GAL2* feedback deletion (GAL2Δ fb) displayed bimodality in the absence of dox. (*B*) *GAL80* feedback deletion (GAL80Δ fb) exhibited bimodal distributions for 0 and 25 ng/mL dox. These concentrations of dox correspond to 40% and 100% of fully induced WT *GAL80* mRNA levels, respectively. (*C*) Comparison of *GAL10* and *TDH3* promoter strengths. Promoters were compared after subtracting the corresponding autofluorescence background (solid red and blue histograms). P_{GAL10} Venus and P_{TDH3} Venus were grown separately in 2% raffinose + 2% galactose or 2% glucose. The autofluorescence background values were obtained from a WT W303a strain lacking a fluorescent reporter grown separately in 2% raffinose or 2% glucose media (dashed red and blue histograms). (*D*) Activation level represents the fraction of high expressing cells for P_{GAL10} and the normalized mean of unimodal distributions for P_{GAL3} and P_{GAL80} (MY; *Materials and Methods*). Lines are fits of the data to Hill functions with Hill coefficients of 3.2, 2.2, and 2 for P_{GAL10}, P_{GAL3}, and P_{GAL80}, respectively. Error bars represent 1 SD (n = 3). (*E*) Representative flow cytometry distributions of Venus from P_{GAL3} and P_{GAL80} for a range of galactose concentrations at steady state. Because the *GAL3* and *GAL80* promoters are weaker than the *GAL10* promoter, the flow cytometry gain settings were increased for these strains to detect the full expression range.

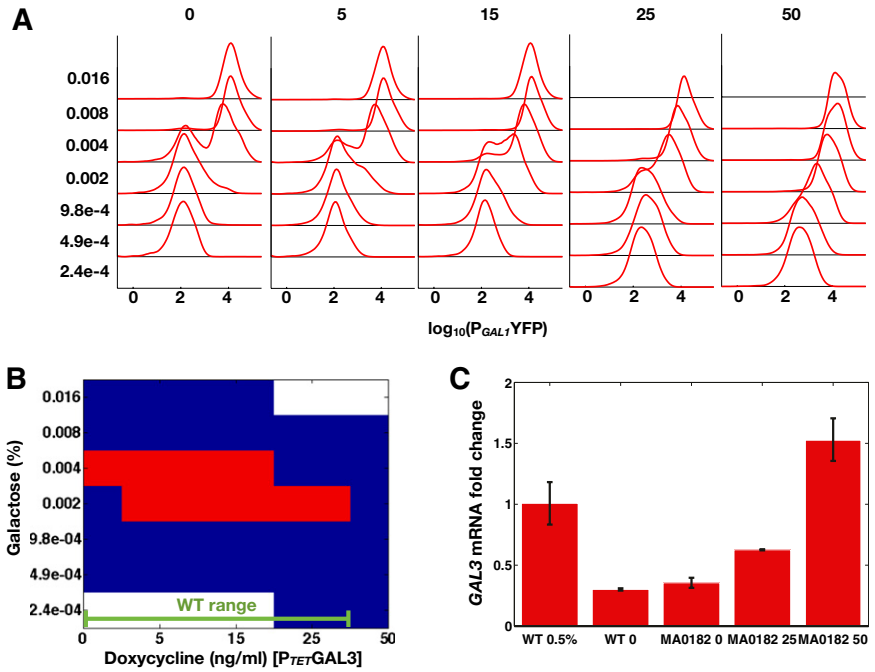

Fig. S2. Experimental characterization of the diploid *GAL3* feedback loop KO strain MA0182 from Acar et al. (5). (*A*) Flow cytometry histograms of YFP fluorescence for a range of dox (horizontal axis) and galactose (percent, vertical axis) concentrations. (*B*) Representation of flow cytometry distributions in *A* as bimodal (red) and unimodal (blue) classified using a Gaussian mixture model algorithm (*Materials and Methods*). The concentrations of galactose that yielded bimodal distributions shifted to lower galactose concentrations as the concentration of *GAL3* was increased, qualitatively reflecting the decrease in the bistability region for the *GAL3* feedback deletion model (Fig. 5*D*). The dose–response was graded for 50 ng/mL dox. The concentrations of dox that map *GAL3* levels in MA0182 to WT expression are indicated by a green line (0-25 ng/mL dox). (*C*) Real-time quantitative PCR measurements comparing *GAL3* mRNA levels in MA0182 with a diploid WT. This WT strain was induced with 0% and 0.5% galactose, and MA0182 was induced with 0, 25, and 50 ng/mL dox. In comparison to WT induced with 0.5% galactose, *GAL3* levels in MA0182 were between 0 (36% with respect to WT) and ~35 ng/mL dox (100% with respect to WT). Error bars represent 1 SD (n = 3).

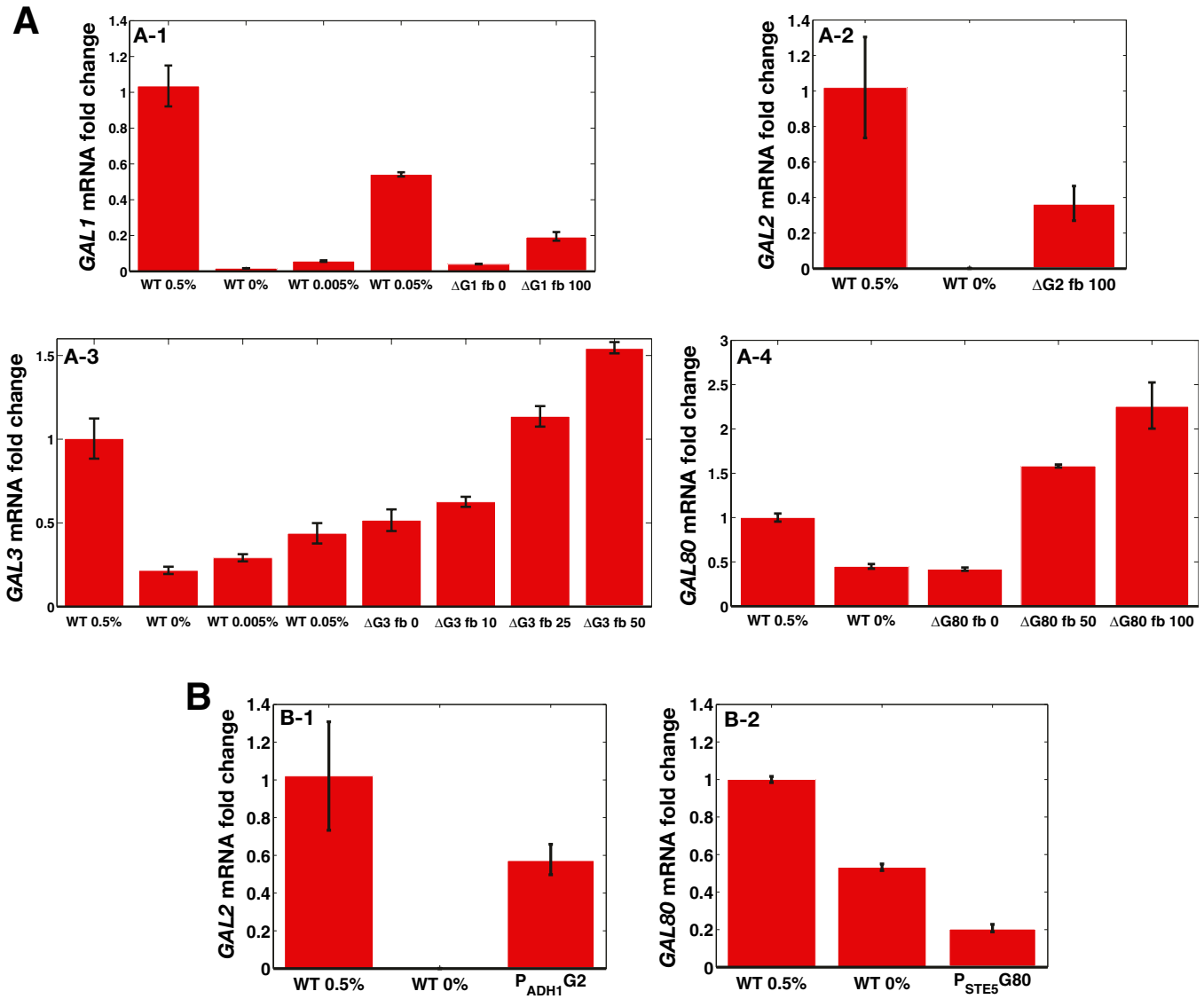

Fig. S3. Real-time quantitative PCR comparing constitutive and WT mRNA levels of *GAL1* (*A1*), *GAL2* (*A2*), *GAL3* (*A3*), and *GAL80* (*A4*). The mRNA expression level for each gene was compared with the corresponding expression level of this gene in WT induced with 0.5% galactose. (*A*) Comparison of *TET* promoter and WT expression ranges. *GAL1* expressed from the *TET* promoter and induced with 0–100 ng/mL was within the range of WT *GAL1* expression. However, P_{TET} GAL1 induced with 0 and 100 ng/mL dox was overexpressed relative to WT induced with 0% and 0.005% galactose, respectively. P_{TET} GAL2 induced with 100 ng/mL dox corresponded to 37% of saturated WT *GAL2* levels. WT *GAL3* levels corresponded to 0–20 ng/mL dox for *GAL3* expressed from the *TET* promoter. However, P_{TET} GAL3 induced with 10 ng/mL dox was overexpressed relative to 0.05% galactose. P_{TET} GAL80 induced with 0–25 ng/mL dox corresponded to WT *GAL80* expression. (*B*) mRNA levels of *GAL2* (*B1*) and *GAL80* (*B2*) regulated by the *ADH1* and *STE5* promoters. *GAL2* and *GAL80* levels were ~58% and 20% of the corresponding gene in WT induced with 0.5% galactose, respectively. Error bars represent 1 SD (n = 3).

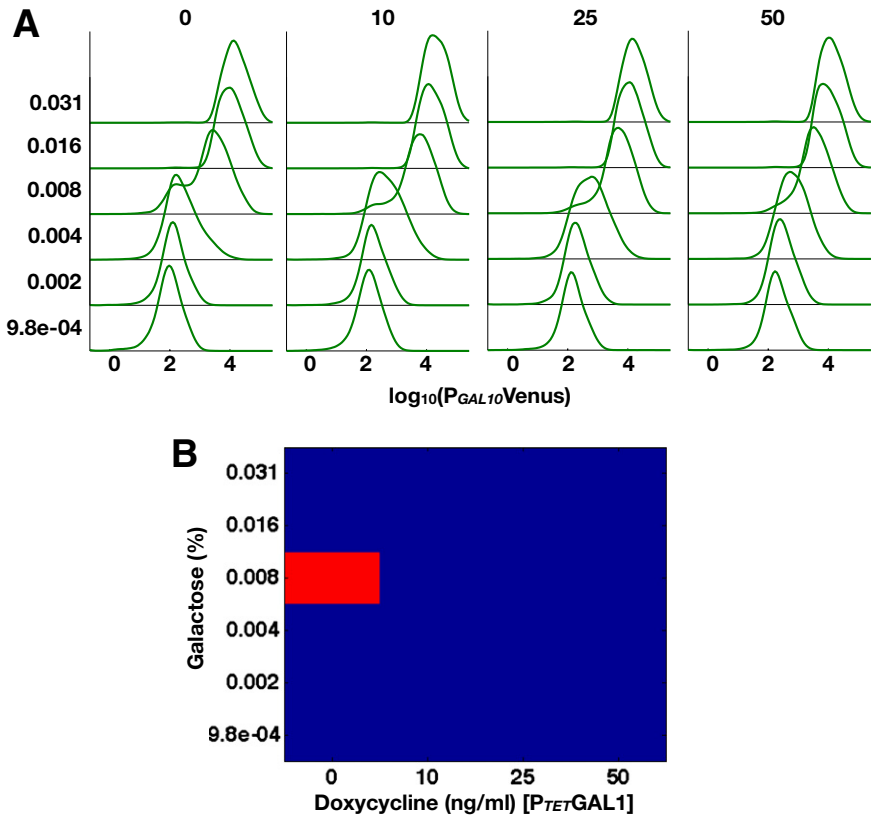

Fig. S4. Experimental characterization of the *GAL1* feedback loop KO strain (GAL1Δ fb). (*A*) Flow cytometry histograms of P_{GAL10} Venus for a range of dox (horizontal axis) and galactose (percent, vertical axis). (*B*) Representation of flow cytometry data in *A* as bimodal (red) and unimodal (blue) determined by a Gaussian mixture model algorithm (*Materials and Methods*). Bimodality was detected for 0 ng/mL dox and vanished for 10, 25, and 50 ng/mL dox.

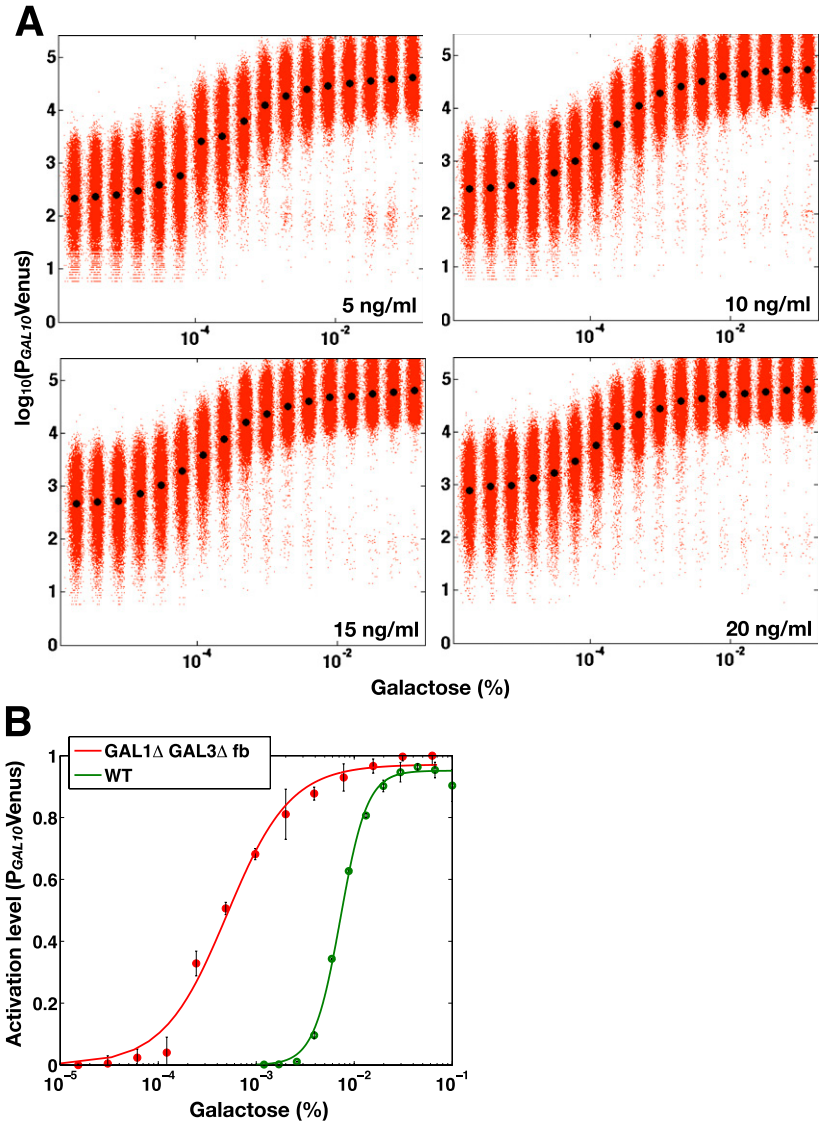

Fig. S5. Deletion of *GAL1* and the *GAL3* feedback loop (GAL1Δ GAL3Δ fb) produced a graded response irrespective of the concentration of *GAL3* and ultrasensitivity is significantly decreased in the absence of *GAL1* and the *GAL3* feedback loop. (*A*) Steady-state flow cytometry measurements of P_{GAL10} Venus in GAL1Δ GAL3Δ fb cells, where *GAL3* was expressed from a *TET* promoter induced with 5, 10, 15, and 20 ng/mL dox. These concentrations of dox correspond to WT *GAL3* levels (Fig. S3*A3*). These measurements were taken on an LSRII analyzer. Each black circle indicates the mean of the distribution determined by a GMM algorithm (*Materials and Methods*). (*B*) Steady-state activation responses of P_{GAL10} Venus in the WT and GAL1Δ GAL3Δ fb. The Hill coefficient for the WT was ~3, whereas the Hill coefficient for GAL1Δ GAL3Δ fb was ~1.3. Each data point for GAL1Δ GAL3Δ fb represents the normalized mean of fluorescence (M_Y; *Materials and Methods*), and the error bars represent 1 SD (n = 3). Each data point for the WT represents the mean of the fraction cells in the high expression state, and the error bars represent 1 SD (n = 3).

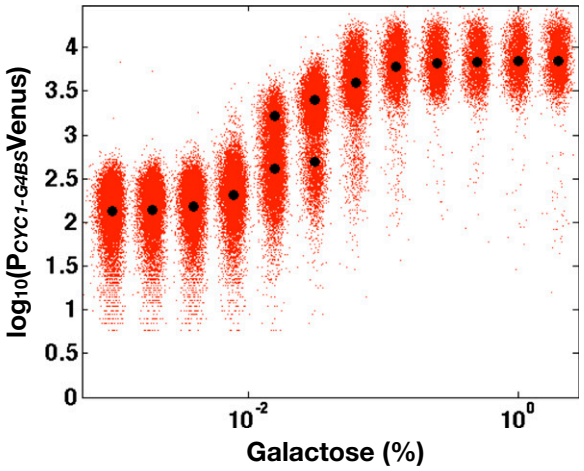

Fig. S6. GAL bimodal response does not require multiple *GAL4* binding sites. A synthetic GAL regulated promoter fusion to Venus with a single *GAL4* binding site was bimodal for two galactose concentrations at steady state. Bimodality was determined using a Gaussian mixture model algorithm (*Materials and Methods*). Black circles represent the means of the fluorescence distributions classified using a Gaussian mixture model (see *Materials and Methods*).

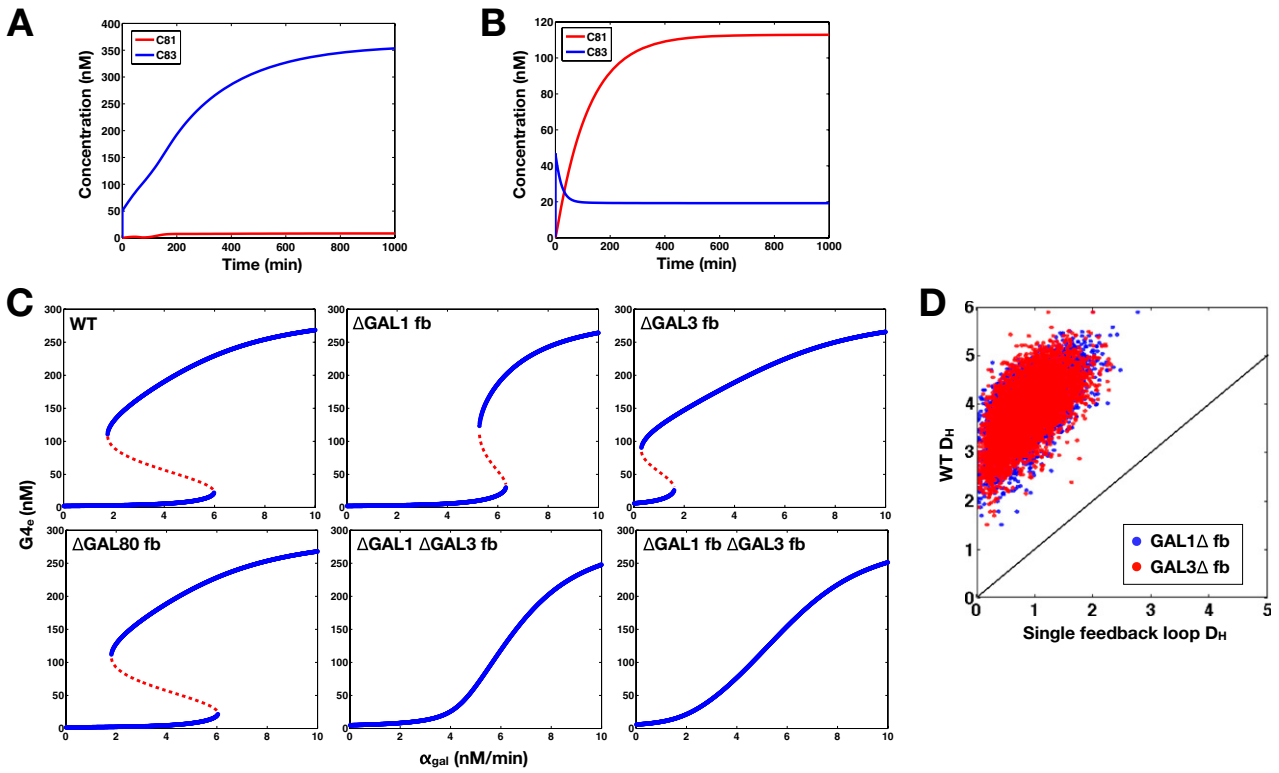

Fig. S7. Parameter set II captures dynamic interplay of Gal1p and Gal3p complex with Gal80p (C81 and C83) and feedback loop KO experimental results. (*A*) Parameter set I indicates that the complex of Gal3p with Gal80p (C83) dominates transiently and at steady state compared with C81 (complex of Gal1p with Gal80p). (*B*) Random parameter sampling (*Materials and Methods*) was used to identify a new parameter set that exhibits transient dominance of the C83 complex and steady-state dominance of the C81 complex. (*C*) Parameter set II qualitatively matches the feedback loop KO experimental data, showing bistability in all feedback loop deletions except the double deletion of *GAL1* and the *GAL3* feedback loop. (*D*) WT model exhibits a larger range of bistability (D_H) compared with the single positive feedback loop systems (*GAL1* and *GAL3*) across a broad region of parameter space ($C_v = 0.1$). Parameter sets I and II are listed in Table S1.

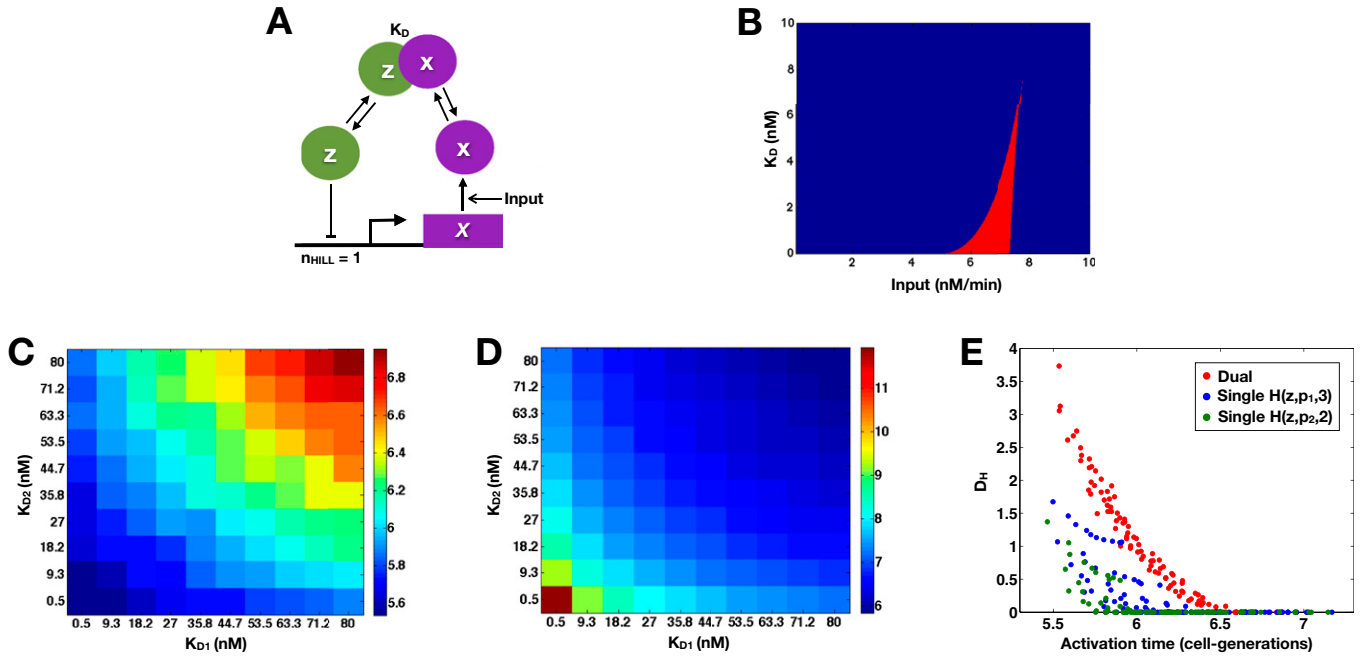

Fig. S8. Molecular sequestration can generate bistability without cooperativity. Relationships between the binding affinities and activation or deactivation response times for the dual feedback loop sequestration model. (*A*) Circuit topology consists of an activator *x* that can form inactive heterodimers with a transcriptional repressor, *z*. The repressor *z* transcriptionally represses the activator *x* with a Hill coefficient of 1 (n_{Hill} = 1, noncooperative). (*B*) Regions of bistability (red) and monostability (blue) for a set of input and K_D values (binding affinity of *x* to *z*). The region of bistability shrinks and eventually disappears as the binding affinity decreases. Model equations and parameter values are listed in section S7. (*C*) Activation response times measured in cell-generations for the double feedback loop sequestration model for different values of K_{D1} and K_{D2}. (*D*) Deactivation response times measured in cell-generations for the double feedback loop sequestration model for different values of K_{D1} and K_{D2}. (*E*) Relationship between activation response times and range of bistability (D_H) for the double positive feedback loop sequestration model for a set of K_{D1} and K_{D2} values. For a fixed nonzero D_H, the double positive feedback loop system could exhibit a faster activation response compared with the single positive feedback loop models.

Table S1. Description of model parameters used in this study

Parameter	Description	Units	Parameter set I*	Parameter set II†
k_{f81}	Forward binding rate of Gal1p to Gal80p	$(nM{\cdot}min)^{-1}$	100	100
k_{r81}	Unbinding rate of Gal1p from Gal80p	Min^{-1}	1,500	2,500
k_{f83}	Forward binding rate of Gal3p to Gal80p	$(nM{\cdot}min)^{-1}$	100	100
k_{r83}	Unbinding rate of Gal3p from Gal80p	Min^{-1}	1	462
k_{f84}	Forward binding rate of Gal4p to Gal80p	$(nM{\cdot}min)^{-1}$	100	100
k_{r84}	Unbinding rate of Gal4p from Gal80p	Min^{-1}	25	1,300
α_{G1}	Gal1p production rate	$nM{\cdot}min^{-1}$	15	35
α_{G3}	Gal3p production rate	$nM{\cdot}min^{-1}$	0.9	8
α_{G4}	Gal4p production rate	$nM{\cdot}min^{-1}$	0.2	3.6
α_{oG80}	Basal Gal80p production rate	$nM{\cdot}min^{-1}$	0.6	5.9
α_{G80}	Gal80p production rate	$nM{\cdot}min^{-1}$	0.9	9
K_{G1}	*GAL1* transcriptional feedback threshold	nM	8	86.7
K_{G3}	*GAL3* transcriptional feedback threshold	nM	8	64.9
K_{G80}	*GAL80* transcriptional feedback threshold	nM	2	1.5
n_1	*GAL1* Hill coefficient	Dimensionless	3	3
n_3	*GAL3* Hill coefficient	Dimensionless	2	2
n_{80}	*GAL80* Hill coefficient	Dimensionless	2	2
γ_{G1}	Gal1p degradation rate	Min^{-1}	0.004	0.0263
γ_{G3}	Gal3p degradation rate	Min^{-1}	0.004	0.004
γ_{G4}	Gal4p degradation rate	Min^{-1}	0.004	0.0119
γ_{G80}	Gal80p degradation rate	Min^{-1}	0.004	0.0073
γ_{C81}	Gal1p-Gal80p (C81) degradation rate	Min^{-1}	0.004	0.0084
γ_{C83}	Gal3p-Gal80p (C83) degradation rate	Min^{-1}	0.004	0.0527
γ_{C84}	Gal4p-Gal80p (C84) degradation rate	Min^{-1}	0.004	0.0177
ε	Scaling factor	Dimensionless	0.1	1.02
α_{G1s}	Constant Gal1p production rate	$nM{\cdot}min^{-1}$	0.1	0.1
α_{G3s}	Constant Gal3p production rate	$nM{\cdot}min^{-1}$	0.1	6
α_{G80s}	Constant Gal80p production rate	$nM{\cdot}min^{-1}$	1.5	13.5

*Original parameter set estimated as described in section S5 (Figs. 4 and 5).
†New parameter set obtained by random parameter sampling (Latin hypercube method) that captures the dynamic interplay of Gal1p and Gal3p (19).

Table S2. Strains used in this study

Strain name	Genotype
WT P_{GAL10} Venus	MATa leu2, trp1::TRP1-P_{GAL10} Venus, ura3, ade2::ADE2, his3
GAL2Δ fb	MATa leu2::LEU2-P_{TEFm4} rtTA-M2, trp1::TRP1-P_{GAL10} Venus, ura3::URA3-P_{TET} GAL2, ade2::ADE2, his3, GAL2Δ ::KAN
GAL3Δ fb	MATa leu2::LEU2-P_{TEFm4} rtTA-M2, trp1::TRP1-P_{GAL10} Venus, ura3::URA3-P_{TET} GAL3, ade2::ADE2, his3, GAL3Δ ::KAN
GAL80Δ fb	MATa leu2::LEU2-P_{TEFm4} rtTA-M2, trp1::TRP1-P_{GAL10} Venus, ura3::URA3-P_{TET} GAL80, ade2::ADE2, his3, GAL80Δ ::HPH
GAL2Δ fb GAL3Δ fb	MATa leu2::LEU2-P_{TEFm4} rtTA-M2, trp1::TRP1-P_{GAL10} Venus, ura3::URA3-P_{TET} GAL3, ade2::ADE2, his3::HIS3-P_{ADH1} GAL2, GAL3Δ ::KAN, GAL2Δ ::NAT
GAL2Δ fb GAL3Δ fb GAL80Δ fb	MATα ura3:URA3-P_{TET} GAL3, leu2::LEU2-$P_{STE\ 5}$ GAL80, ade2::ADE2-P_{GAL10} Venus, trp1::TRP1-P_{ADH1} GAL2, his3::HIS3-P_{TEFm4} rtTA-M2, GAL3Δ ::KAN, GAL2Δ ::NAT, GAL80Δ ::HPH
GAL1Δ *	MATα leu2, trp1::TRP1-P_{GAL10} Venus, ura3, ade2::ADE2, his3, GAL1Δ
GAL1Δ * fb	MATα leu2::LEU2-P_{TEFm4} rtTA-M2, trp1::TRP1-P_{GAL10} Venus, ura3, ade2::ADE2, his3, GAL1Δ
GAL1Δ * GAL2Δ fb	MATα leu2::LEU2-P_{TEFm4} rtTA-M2, trp1::TRP1-P_{GAL10} Venus, ura3::URA3-P_{TET} GAL2, ade2::ADE2, his3, GAL2Δ ::NAT, GAL1Δ
GAL1Δ * GAL3Δ fb	MATα leu2::LEU2-P_{TEFm4} rtTA-M2, trp1::TRP1-P_{GAL10} Venus, ura3::URA3-P_{TET} GAL3, ade2::ADE2, his3, GAL3Δ ::KAN, GAL1Δ
GAL1Δ * GAL80Δ fb	MATα leu2::LEU2-P_{TEFm4} rtTA-M2, trp1::TRP1-P_{GAL10} Venus, ura3::URA3-P_{TET} GAL3, ade2::ADE2, his3, GAL80Δ ::HPH, GAL1Δ
WT P_{GAL3} Venus	MATa leu2, trp1::TRP1-P*GAL3* Venus, ura3, ade2::ADE2, his3
WT P_{GAL80} Venus	MATa leu2, trp1::TRP1-P_{GAL80} Venus, ura3, ade2::ADE2, his3
WT P_{TDH3} Venus	MATa leu2, trp1::TRP1-P_{TDH3} Venus, ura3, ade2::ADE2, his3
WT $P_{CYC1–G4BS}$ Venus	MATa leu2, trp1::TRP1-$P_{CYC1\text{-}G4BS}$ Venus, ura3, ade2::ADE2, his3
WT diploid	MATa/α leu2/leu2::LEU2-P_{TEFm4} rtTA-M2, trp1::TRP1-P_{GAL10} Venus/trp1, ura3/ura3, ade2::ADE2/ade2, his3/his3
MA0182†	MATa/α, ura3/ura3::URA3-P_{TET02} GAL3, his3::HIS3/his3, ade2::ADE2-P_{MYO2} rtTA/ade2::ADE2-P_{GAL1} YFP, GAL3Δ ::KAN/GAL3Δ ::KAN

All strains were W303. rtTA, reverse mutant of the transcription factor TetR.
*Constructed using CSY53 background described by Hawkins and Smolke (1).
†Strain described by Acar et al. (2).

1. Hawkins KM, Smolke CD (2006) The regulatory roles of the galactose permease and kinase in the induction response of the GAL network in Saccharomyces cerevisiae. *J Biol Chem* 281 (19):13485–13492.
2. Acar M, Becskei A, van Oudenaarden A (2005) Enhancement of cellular memory by reducing stochastic transitions. *Nature* 435(7039):228–232.